Journal of Power Sources 196 (2011) 6214–6218

Contents lists available at ScienceDirect

Journal of Power Sources

journal homepage: www.elsevier.com/locate/jpowsour

Short communication

Thin film nanocrystalline $Ba_{0.5}Sr_{0.5}Co_{0.8}Fe_{0.2}O_3$: Synthesis, conductivity, and micro-solid oxide fuel cells

Kian Kerman*, Bo-Kuai Lai, Shriram Ramanathan

Harvard School of Engineering and Applied Sciences, Harvard University, Cambridge, MA 02138, USA

ARTICLE INFO

Article history:
Received 6 February 2011
Received in revised form 16 March 2011
Accepted 23 March 2011
Available online 31 March 2011

Keywords:
Micro-solid oxide fuel cell
BSCF
Nanocrystalline
Conductivity
Thin films

ABSTRACT

We report on single phase polycrystalline $Ba_{0.5}Sr_{0.5}Co_{0.8}Fe_{0.2}O_3$ thin films grown on (100) $(Y_2O_3)_{0.08}(ZrO_2)_{0.92}$ substrates by radio frequency sputtering. Detailed studies on electrical conductivity as a function of temperature up to 500 °C are carried out for films in the 20–100 nm thickness range. Free-standing thin film micro-solid oxide fuel cells utilizing nanostructured $Ba_{0.5}Sr_{0.5}Co_{0.8}Fe_{0.2}O_3$ cathodes are fabricated and tested for the first time. A maximum power density of 35 mW cm^{-2} at 520 °C was obtained with $Ba_{0.5}Sr_{0.5}Co_{0.8}Fe_{0.2}O_3/(Y_2O_3)_{0.08}(ZrO_2)_{0.92}$/Pt micro-solid oxide fuel cells. These results indicate the significance of microstructure on electrical properties of $Ba_{0.5}Sr_{0.5}Co_{0.8}Fe_{0.2}O_3$ and present the first successful thin film micro-solid oxide fuel cells integrating $Ba_{0.5}Sr_{0.5}Co_{0.8}Fe_{0.2}O_3$. We anticipate these results to be of relevance in advancing micro-solid oxide fuel cells for reduced temperature operation with dense oxide cathodes.

1. Introduction

Currently, there is a tremendous effort to reduce the operating temperature of solid oxide fuel cells (SOFCs). High temperature operation (800–1000 °C) is beneficial in enhancing the electrode reaction kinetics and reducing ohmic resistance across the electrolyte; however, it also increases the possibility of parasitic reactions between cell components, requires high cost metallic interconnects, and creates sealing difficulty for stacking architectures. Reducing SOFC operation temperature is seen as a method to address the aforementioned shortcomings. To counteract the increased ohmic resistance across the electrolyte during reduced temperature operation, micro-SOFCs (μSOFCs) utilizing thin film electrolytes are being actively developed though many utilize Pt as both the anode and cathode [1–5].

A significant challenge for high performance μSOFCs operating at reduced temperatures ($T \leq 600$ °C) is developing stable electrode materials that have sufficient electronic and ionic conductivity, as well as high catalytic activity [6]. In this regard, perovskite oxides that exhibit mixed conduction behavior have been shown to be some of the most promising cathode candidates [7,8]. Thin film mixed electronic-ionic conductors offer the benefit of extending the triple phase boundary (TPB) of SOFC devices to the entire plane of the cathode electrolyte interface. Recently, Shao and Haile reported a novel oxide electro-catalyst, namely $Ba_{0.5}Sr_{0.5}Co_{0.8}Fe_{0.2}O_{3-\delta}$ (BSCF), which exhibits high power densities down to 400 °C [9]. BSCF is based on A-site substitution of Ba^{2+} into $SrCo_{0.8}Fe_{0.2}O_{3-\delta}$. The advantages of this substitution include phase stability, i.e., BSCF does not order into a brown-millerite phase, a higher oxygen vacancy concentration, and suitable electronic conductivity [9–11].

Though the material has received much attention in bulk, reports of thin film BSCF conductivity are limited [12–14]. Burriel et al. [14] reported the electrical conductivity of epitaxial thin film BSCF measured by 2-probe method to be ~45 S cm^{-1} at 400 °C, with activation energy of 0.254 eV in the 30–300 °C range and 0.182 eV in the 300–900 °C range in air. To the best of our knowledge, there has been no demonstration of thin film based SOFCs integrating BSCF cathodes, though other complex oxide cathodes have been recently been investigated [5,15] exhibiting power density of the order or 100 mW cm^{-2} near 550 °C. Experimental challenges in these regards include synthesis of dense single phase nanostructured oxide films that possess mechanical integrity with good electrical properties. In this study, we report the high temperature electrical properties of dense nanocrystalline BSCF thin films synthesized by radio frequency sputtering. Additionally, we demonstrate the first free standing thin film μSOFC incorporating dense 100 nm thick nanocrystalline BSCF cathode.

2. Experimental

BSCF thin films were grown at a power of 90 W by radio frequency (RF) sputtering from a stoichiometric target in 5 mTorr of Ar at a substrate temperature of 550 °C. Care was taken to grow the

* Corresponding author. Tel.: +1 609 638 6139.
E-mail address: kkerman@fas.harvard.edu (K. Kerman).

0378-7753/$ – see front matter © 2011 Elsevier B.V. All rights reserved.
doi:10.1016/j.jpowsour.2011.03.049

films without loss of mechanical integrity in the precursor sputter target. X-ray reflectivity (XRR) was used to determine the thickness and growth rate of the films. The conditions above yielded a growth rate of 1 nm min^{-1} and were used to fabricate the various samples in this study. Glancing incidence angle X-ray diffraction (XRD) was performed using Bruker D8 Discover instrument. Scans were taken at an incidence angle of 1° in omega, using a step size of 0.02° s^{-1} with a Cu Kα source at 40 kV and 40 mA. Plan view transmission electron microscope (TEM) samples were prepared by manual polishing followed by ion milling to electron transparency using a Fischione 10-10 dual-beam ion mill. A JEOL 2100 TEM was used to investigate the structure and grain size of the BSCF films.

Pt electrodes for conductivity measurements were deposited at a power of 250 W through a shadow mask by direct current sputtering without substrate heating at an Ar pressure of 4 mTorr. Lateral conductivity was calculated from 2-probe *I–V* measurements in air from room temperature up to 500 °C at a heating and cooling rate of 2 °C min^{-1}. μSOFC devices incorporating BSCF cathodes were fabricated by patterning Si_3N_4 coated Si wafers using photolithography. The patterned wafers were then selectively wet etched in a KOH solution to reveal a free standing Si_3N_4 structure. The electrolyte and cathode were grown on this structure prior to final removal of the Si_3N_4 and deposition of the Pt anode. More detail on this fabrication method is discussed in previous works [4,5,16]. The $(Y_2O_3)_{0.08}(ZrO_2)_{0.92}$ (YSZ) electrolyte was grown by RF sputtering at a power of 100 W from a stoichiometric target in 5 mTorr Ar at substrate temperature of 550 °C. Porous Pt was deposited at a power of 250 W without substrate heating at a pressure of 75 mtorr. μSOFC testing was performed in a custom test station [4] using a mixture of 97% fuel and 3% H_2O and air as the oxidant. Fuel was fed at a rate of 150 ml min^{-1} and comprised of an Ar carrier gas with 5% H_2.

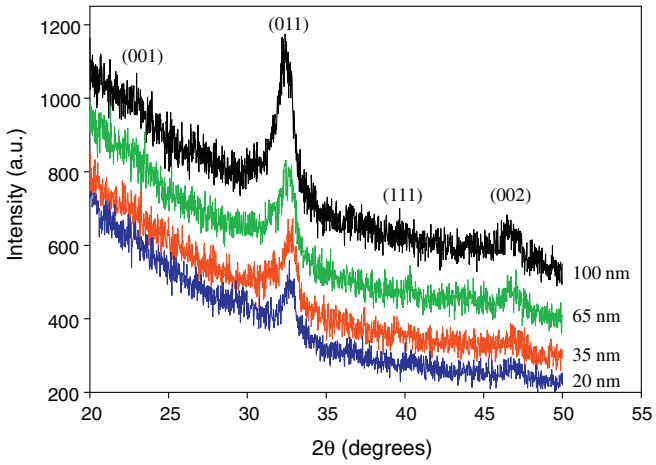

Fig. 1. Glancing incidence X-ray diffraction pattern of sub-100 nm BSCF thin films grown on (1 0 0) YSZ, with peaks indexed in accordance with JCPDS 055-0563.

3. Results and discussion

3.1. Thin film BSCF structural and conductivity studies

The glancing incidence XRD patterns of BSCF films grown on (1 0 0) YSZ substrate shown in Fig. 1 matches well to JCPDS 055-0563, confirming the films are single phase and polycrystalline. It can be seen that the films exhibit a (0 1 1) preferred orientation, which is further corroborated by the selected area transmission electron diffraction (SAED) pattern shown in Fig. 2d. Lateral conductivity of bare single crystalline YSZ substrates indicated a

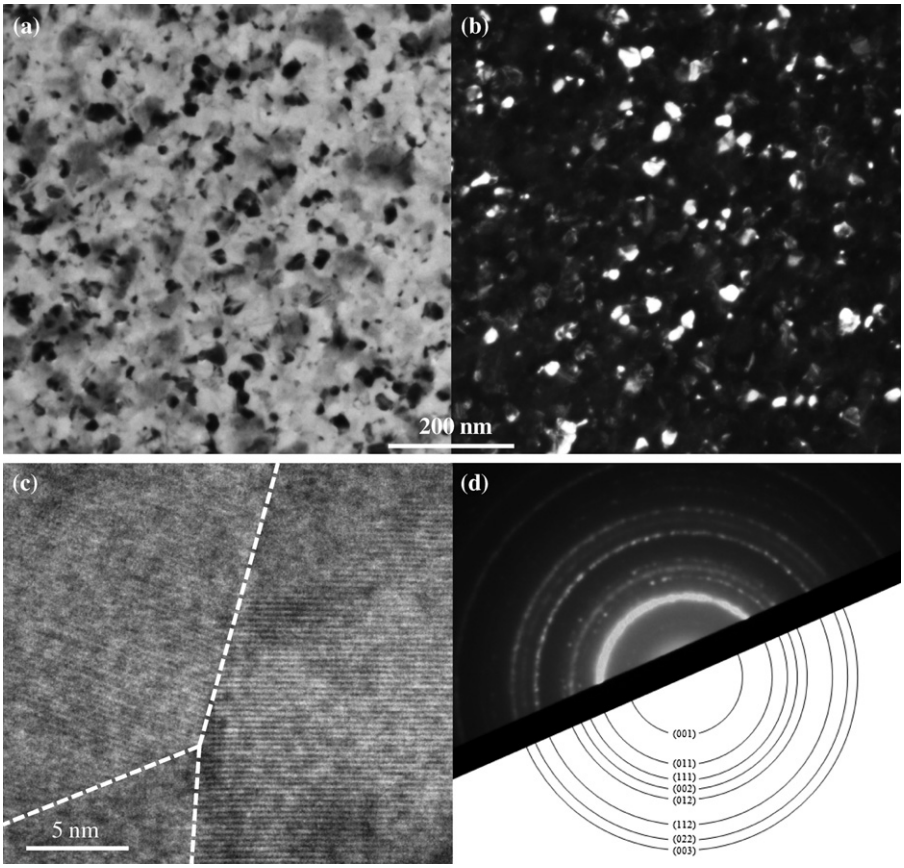

Fig. 2. (a) Bright field, (b) dark field, (c) high resolution plan view TEM images of BSCF thin films, and (d) indexed selected area diffraction pattern showing dense nanocrystalline microstructure.

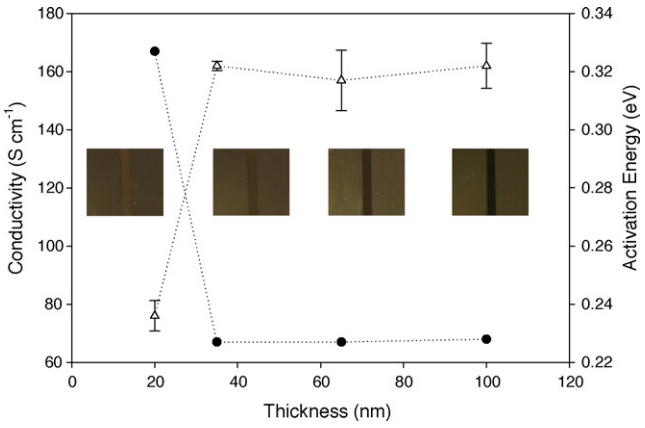

Fig. 3. Plot of electrical conductivity (σ) at 400 °C and activation energy (E_a) as a function of thickness. Open and closed symbols represent σ and E_a, respectively. The inset shows optical micrographs of the films.

negligible contribution to BSCF thin film conduction properties. Bright and dark field plan view TEM images in Fig. 2 depict the nano-granular polycrystalline nature of the BSCF films. The average grain size was estimated to be ~25 nm. A high resolution TEM image in Fig. 2 shows the dense polycrystalline structure with no amorphous intergranular regions, while the SAED pattern confirms single phase, textured nature of the film.

Fig. 3 shows the thickness dependence of lateral electrical conductivity at 400 °C. Contact resistance was not directly corrected for; however, resistivity at room temperature using a 4-point probe method was equivalent to 2-probe measurements. Absolute values of conductivity can slightly increase as a result of any non-negligible contact resistance, but the trend presented should remain. Activation energy (E_a) was calculated from cooling curves of an Arrhenius plot in Fig. 4, which exhibits near linear behavior between 400 °C and 200 °C. In this temperature range, small polaron hopping conduction associated with the mixed-valent Co and Fe sites is believed to govern electrical conductivity [17,18] by the following relationship:

$$\sigma = \left(\frac{A}{T}\right) e^{\left(\frac{-E_a}{kT}\right)}$$

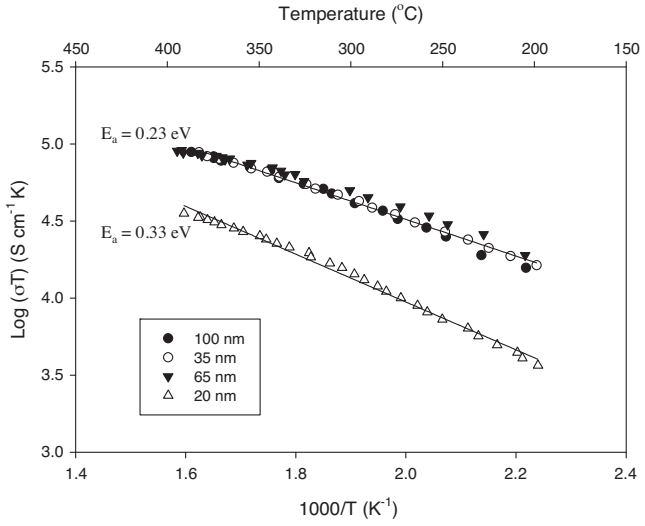

Fig. 4. Arrhenius plot used to calculate the activation energy upon cooling in the 400–200 °C range. Coefficient of determination on linear fits were accurate to better than 0.995.

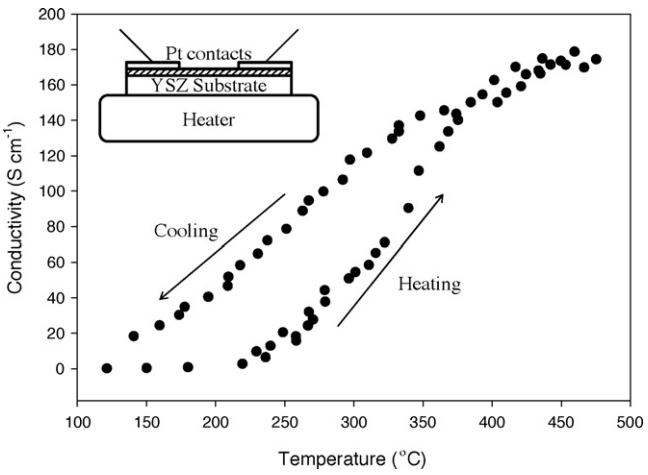

Fig. 5. Lateral electrical conductivity of a 100 nm BSCF thin film measured at a heating and cooling rate of 2 °C min^{-1}. The inset shows a schematic of the measurement set-up.

where σ is electrical conductivity, A is a material specific constant, k is the Boltzmann constant, and T is the absolute temperature. Above 400 °C, the trend in conductivity with increasing temperature begins to saturate, indicating the emergence of oxygen vacancies inhibiting polaron transport; consistent with what has been reported in the case of bulk BSCF, where metal-like conduction behavior is seen above this temperature [17,18]. These two regimes can be seen more clearly in the conductivity plot as a function of temperature shown in Fig. 5 for a 100 nm thick sample. The slight variation between heating and cooling curves is likely due to BSCF approaching its equilibrium oxygen stoichiometry at a rate slower than that which temperature was being ramped. Unlike thin films of purely ionic conductors such as $(Y_2O_3)_x(ZrO_2)_{1-x}$, where space charge effects at interfaces have shown to significantly alter lateral ionic conduction as a function of film thickness [19,20]; the electronic conduction in mixed conducting BSCF does not appear to show a noticeable trend in the limit when film thickness exceeds grain size. In this limit, E_a observed in nanocrystalline BSCF films is similar to that recently reported for epitaxial BSCF films [14], while conductivity in nanocrystalline films is approximately twice as high, pointing to the significance of microstructure for electronic transport. Microstructural significance on the nano-scale could be related total carrier concentration. The electrical conductivity of the nanocrystalline BSCF thin films presented here is comparable to nanocrystalline oxide cathode $La_{0.6}Sr_{0.4}Co_{0.8}Fe_{0.2}O_3$ films grown by similar methods [21].

3.2. μSOFCs incorporating thin film BSCF

μSOFCs were fabricated using porous Pt as the anode, dense 100 nm YSZ as the electrolyte, and dense BSCF as the cathode. μSOFCs with 35, 50, and 100 nm thick BSCF cathodes were fabricated and tested. The maximum power density of such cells decreased monotonically with decreasing cathode thickness. A schematic of the final free standing tri-layer structure is shown in Fig. 6, while the maximum power density of μSOFCs with 100 nm

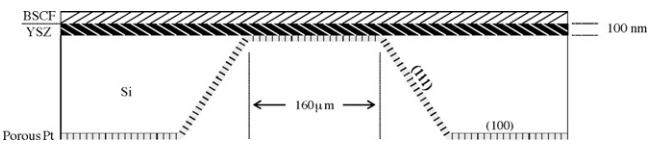

Fig. 6. Schematic of free standing BSCF/YSZ/Pt μSOFCs fabricated in this study.

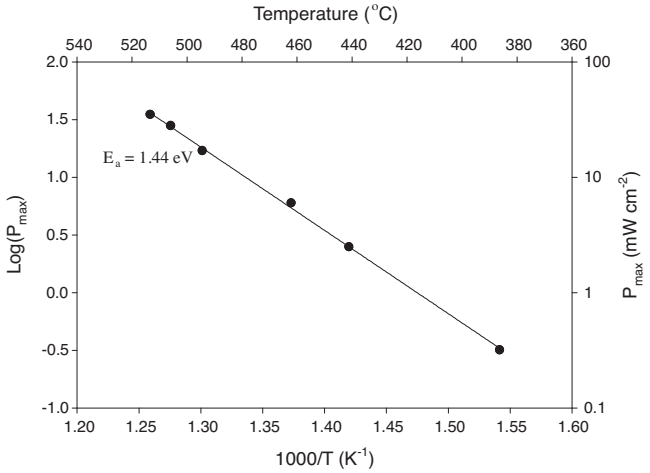

Fig. 7. Arrhenius plot of the maximum power density of 100 nm BSCF/YSZ/Pt μSOFCs as a function of temperature exhibiting clear linear behavior with a coefficient of determination above 0.999.

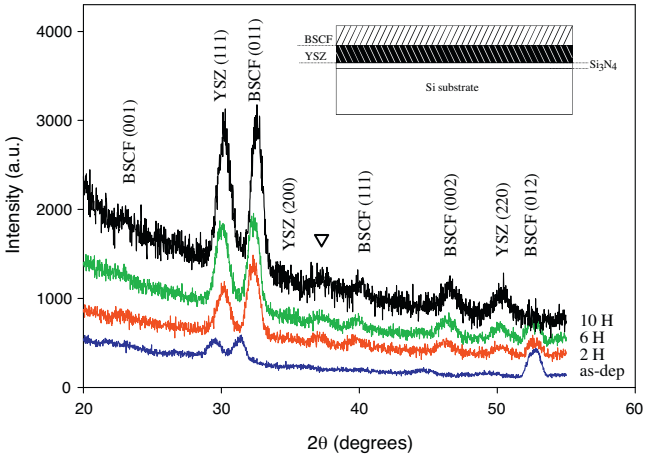

Fig. 9. Glancing incidence XRD patterns of a BSCF/YSZ thin film structure as deposited and annealed at 600 °C for various times. BSCF and YSZ reflections are indexed to JCPDS 055-0563 and 030-1468, respectively. The ▽ symbol represents the emergence of an unidentified phase, while the inset shows a schematic of the film structure.

BSCF as a function of temperature is plotted in Fig. 7. Using a linear fit to the Arrhenius plot in Fig. 7, overall activation energy of the maximum power density for the μSOFCs was estimated to be 1.44 eV. Ionic transport through YSZ electrolytes generally occurs with an activation barrier of ~1 eV [19,20], while the kinetics of oxygen reduction on the surface of BSCF has been observed to occur with an activation energy in the 1.4–1.7 eV range [22,23]. Therefore, it is reasonable to infer that thin film BSCF cathodes are likely dominating the overall performance attributes in the μSOFCs presented in this report. The total area specific resistance of BSCF/YSZ/Pt cell at 520 °C was found to be 2.7 Ω cm^2, which is about 25 times higher than that of Pt/YSZ/Pt cells at similar temperatures [16]. Since these two μSOFCs differ only in the cathode material, performance can be expected to be similarly lower. The current–voltage characteristics at the maximum power density for μSOFCs with 100 nm thick BSCF cathodes are shown in Fig. 8. A maximum power density of 35 mW cm^{-2} was achieved at 520 °C. The Nernst potential under measurement conditions at 520 °C should be 1.08 V, however an open circuit potential (OCV) of 0.63 V was observed. In light of previously reported Pt/YSZ/Pt μSOFCs exhibiting near ideal OCVs, even with electrolytes as thin as 27 nm [16], and knowing that BSCF reaction kinetics are dominating the performance, it is likely that the OCV deviation is due to poor catalytic activity towards oxygen reduction at these temperatures. It should be noted that reports

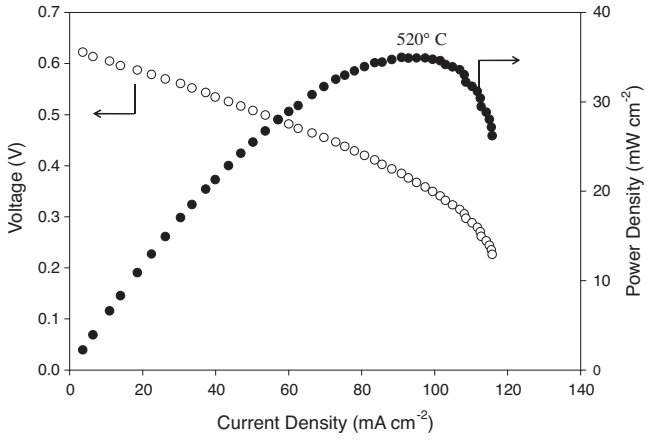

Fig. 8. Current–voltage (*I–V*) characteristics of the 100 nm BSCF/YSZ/Pt μSOFC at 520 °C. Open and closed symbols represent voltage and power density, respectively.

utilizing oxide cathodes in μSOFCsoften show an OCV below the ideal thermodynamic potential [15,24,25]. This issue is commonly addressed by integrating a current collector atop the cathode. Metals used for this purpose provide a less resistive path for electrons to be externally drawn or supplied and can potentially contribute to the catalytic activity towards oxygen reduction, which would increase the observed OCV.

Since the activation barrier for the μSOFC points to the significance of BSCF, influencing factors such as annealing effects and surface vacancies were considered. XRD patterns of annealed BSCF/YSZ thin film structures on Si_3N_4/Si substrate at 600 °C in air for various lengths of time are shown in Fig. 9. The pattern shows the onset of a small unidentified peak around ~37° 2θ, which possibly hints at a parasitic reaction at the cathode/electrolyte interface. Reaction products with YSZ and structural meta-stability of the cubic phase of BSCF have been observed after extended high temperature annealing conditions [26–29]; however there have been no investigations into stability in the sub-600 °C regime, especially in such ultra-thin films. Fig. 8 also shows a shift towards higher 2θ for the (011) BSCF peak under post-deposition annealing conditions. Such a trend indicates the incorporation of oxygen into the lattice. The increased anion concentration exerts an electrostatic attraction amongst its neighboring cations, contracting the unit cell volume. In other words, by introducing oxygen into the lattice, the oxidation state of the neighboring cations increases and likely reduces the cationic radius, decreasing the unit cell volume and hence d-spacing, shifting the XRD pattern to higher 2θ values. Similar behavior has been observed in other complex perovskite oxide films grown in a reducing atmosphere [21,30].

Conventional SOFCs may employ porous electrode structures to facilitate oxygen transport to reaction sites, whereas the μSOFCs reported here utilize a dense cathode, limiting reaction sites for oxygen reduction to the surface of BSCF. Extensive studies on BSCF micro-electrodes point to the significance of oxygen vacancies at the surface in facilitating fast reaction rates and low area specific resistance [22,23]. As a result, oxygen incorporation into vacant surface BSCF sites may influence the overall kinetic processes governing performance as a stable cathode for extended periods of time. Nevertheless, we note that the first successful demonstration of such a fuel cell is promising for advancing investigation into new, stable oxides for low temperature SOFCs. Performance presented here is in the range of power output seen with other dense nanos-

tructured oxide cathodes such as $La_{0.6}Sr_{0.4}Co_{0.8}Fe_{0.2}O_3$ deposited by similar physical vapor deposition techniques [5,15].

4. Conclusion

We have shown that electrical conduction in dense nanocrystalline thin films of BSCF is thickness independent in the sub-100 nm range in the limit where film thickness exceeds grain size. Further, the activation energy for conduction in this limit, ~0.23 eV, is consistent with reported values for BSCF indicating a similar conduction mechanism. The slightly enhanced conductivity in nanocrystalline thin films compared to epitaxial films and bulk ceramics point to the significance of microstructural effects. Free standing thin film μSOFCs were fabricated with 100 nm thick nanocrystalline BSCF cathodes for the first time and showed a maximal performance of 35 mW cm^{-2} at 520 °C. We anticipate these results on nanostructured thin film BSCF could be of relevance to advancing the development of stable low temperature thin film solid oxide fuel cells.

Acknowledgment

The authors acknowledge National Science Foundation Grant #CCF-0926148 for financial support.

References

[1] S. de Souza, S.J. Visco, L.C. De Jonghe, Solid State Ionics 98 (1997) 57–61.
[2] A. Evans, A. Bieberle-Hütter, J.L.M. Rupp, L.J. Gauckler, J. Power Sources 194 (2009) 119–129.
[3] H. Huang, M. Nakamura, P.C. Su, R. Fasching, Y. Saito, F.B. Prinz, J. Electrochem. Soc. 154 (2007) B20–B24.
[4] U.P. Muecke, D. Beckel, A. Bernard, A. Bieberle-Hütter, S. Graf, A. Infortuna, P. Müller, J.L.M. Rupp, J. Schneider, L.J. Gauckler, Adv. Funct. Mater. 18 (2008) 3158–3168.
[5] A.C. Johnson, B.-K. Lai, H. Xiong, S. Ramanathan, J. Power Sources 186 (2009) 252–260.
[6] B.-K. Lai, K. Kerman, S. Ramanathan, J. Power Sources 196 (2011) 1826–1832.
[7] J. Richter, P. Holtappels, T. Graule, T. Nakamura, L.J. Gauckler, Monatsh. Chem. 140 (2009) 985–999.
[8] D.J.L. Brett, A. Atkinson, N.P. Brandon, S.J. Skinner, Chem. Soc. Rev. 37 (2008) 1568–1578.
[9] Z. Shao, S.M. Haile, Nature 431 (2004) 170–173.
[10] Z.P. Shao, W.S. Yang, Y. Cong, H. Dong, J.H. Tong, G.X. Xiong, J. Membr. Sci. 172 (2000) 177.
[11] W. Zhou, R. Ran, Z. Shao, J. Power Sources 192 (2009) 231–246.
[12] L. Wang, R. Merkle, G. Cristiani, B. Stuhlhofer, H. Habermeier, J. Maier, ECS Trans. 13 (2008) 85–95.
[13] L. Wang, R. Merkle, J. Maier, T. Acartürk, U. Starke, Appl. Phys. Lett. 94 (2009) 071908.
[14] M. Burriel, C. Niedrig, W. Menesklou, S.F. Wagner, J. Santiso, E. Ivers-Tiffée, Solid State Ionics 181 (2010) 602–608.
[15] B.-K. Lai, K. Kerman, S. Ramanathan, J. Power Sources 195 (2010) 5185–5196.
[16] K. Kerman, B.-K. Lai, S. Ramanathan, J. Power Sources 196 (2011) 2608–2614.
[17] B. Wei, Z. Lü, S. Li, Y. Liu, K. Liu, W. Su, Electrochem. Solid-State Lett. 8 (2005) A428–A431.
[18] Z. Yáng, A.S. Harvey, A. Infortuna, J. Schoonman, L.J. Gauckler, J. Solid State Electrochem. (2010), doi:10.1007/s10008-010r-r1208-4.
[19] I. Kosacki, C.M. Rouleau, P.F. Becher, J. Bentley, D.H. Lowndes, Electrochem. Solid-State Lett. 7 (2004) A459–A461.
[20] A. Karthikeyan, C.L. Chang, S. Ramanathan, Appl. Phys. Lett. 89 (2006) 183116.
[21] B.-K. Lai, A.C. Johnson, H. Xiong, S. Ramanathan, J. Power Sources 186 (2009) 115–122.
[22] F.S. Baumann, J. Fleig, G. Cristiani, B. Stuhlhofer, H.-U. Habermeier, J. Maier, J. Electrochem. Soc. 154 (2007) B931–B941.
[23] L. Wang, R. Merkle, J. Maier, J. Electrochem. Soc. 157 (2010) B1802–B1808.
[24] A. Ignatiev, X. Chen, N.J. Wu, Z.G. Lu, L. Smith, Dalton Trans. 40 (2008) 5501–5506.
[25] S. Rey-Mermet, Y. Yan, C. Sandu, G. Deng, P. Muralt, Thin Solid Films 518 (2010) 4743–4746.
[26] Z. Duan, M. Yang, A. Yan, Z. Hou, Y. Dong, Y. Chong, M. Cheng, W. Yang, J. Power Sources 160 (2006) 57–64.
[27] S. Svarcová, K. Wiik, J. Tolchard, H.J.M. Bouwmeester, T. Grande, Solid State Ionics 178 (2008) 1787–1791.
[28] D.N. Mueller, R.A. De Souza, T.E. Weirich, D. Roehrens, J. Mayer, M. Martin, Phys. Chem. Chem. Phys. 12 (2010) 10320–10328.
[29] K. Efimov, Q. Xu, A. Feldhoff, Chem. Mater. 22 (2010) 5866–5875.
[30] A. Podpirka, M.W. Cole, S. Ramanathan, Appl. Phys. Lett. 92 (2008) 212906.